Nonlinear multicontrast microscopy of hematoxylin-and-eosin-stained histological sections

Adam Tuer
Danielle Tokarz
Nicole Prent
Richard Cisek
University of Toronto
Department of Physics
Institute for Optical Sciences
Department of Chemical and Physical Sciences
3359 Mississauga Road North
Mississauga, Ontario, L5L 1C6 Canada

Jennifer Alami
Daniel J. Dumont
Ludmila Bakueva
John Rowlands
University of Toronto
Sunnybrook Health Sciences Centre
Department of Medical Biophysics
610 University Avenue
Toronto, Ontario M5G 2M9, Canada

Virginijus Barzda
University of Toronto
Department of Physics
Institute for Optical Sciences
Department of Chemical and Physical Sciences
3359 Mississauga Road North
Mississauga, Ontario, L5L 1C6 Canada

Abstract. Imaging hematoxylin-and-eosin-stained cancerous histological sections with multicontrast nonlinear excitation fluorescence, second- and third-harmonic generation (THG) microscopy reveals cellular structures with extremely high image contrast. Absorption and fluorescence spectroscopy together with second hyperpolarizability measurements of the dyes shows that strong THG appears due to neutral hemalum aggregation and is subsequently enhanced by interaction with eosin. Additionally, fluorescence lifetime imaging microscopy reveals eosin fluorescence quenching by hemalums, showing better suitability of only eosin staining for fluorescence microscopy. Multicontrast nonlinear microscopy has the potential to differentiate between cancerous and healthy tissue at a single cell level. [DOI: 10.1117/1.3382908]

Keywords: medical imaging; multiphoton processes; nonlinear optics; nonlinear image processing; scanning microscopy; tissues.

Paper 09400RR received Sep. 10, 2009; revised manuscript received Feb. 5, 2010; accepted for publication Feb. 22, 2010; published online Apr. 28, 2010.

1 Introduction

Hematoxylin and eosin (H&E) staining is commonly referred to as one of the most popular methods for pathologists to perform on histological sections for the purposes of medical diagnostics. This staining method has been used for the better part of the last century due to its simplicity and ability to adequately contrast cell nuclei from the cytoplasm and extracellular structures and currently is referred to as the gold standard for histological investigations.[1] Visualization of H&E stained samples is usually performed with white light microscopy. Unfortunately, white light microscopy requires thin sectioning of the tissue and, therefore, three-dimensional (3-D) structure can be reconstructed only after tedious imaging of consecutive sections. Thus, an improved visualization, which provides faster imaging, 3-D structural information, as well as greater spatial resolution with higher image contrast, is highly desirable for pathological investigations.

Nonlinear multicontrast laser scanning microscopy is a novel technique that utilizes a high photon flux density provided by ultrafast lasers.[2] At the focus of a microscope objective, the laser-induced nonlinear light-matter interactions that simultaneously generate multiphoton excitation fluorescence (MPF), second-harmonic generation (SHG), and third-harmonic generation (THG) are used as structural visualization contrast mechanisms.[3] The nonlinear signals are confined to the focal volume, thus allowing for submicrometer resolution optical sectioning of tissue slices a few hundred micrometers thick. However, an essential requirement for successful nonlinear imaging of stained tissue is that the dyes are readily visualized by the nonlinear contrast mechanisms. Dyes, which exhibit strong nonlinear properties, in particular, related to harmonic generation, have been termed as harmonophores.

The H&E method employs the use of two dyes: (H) hematoxylin and (E) eosin. There are multiple staining procedures available, mostly differing in the composition of the H solution. In Harris hematoxylin staining, histological sections are first stained with H (Harris formula), which contains hematoxylin, an oxidizing agent, ammonium alum dissolved in ethanol, and deionized water.[1] Hematoxylin is oxidized, with the aid of sodium iodate, into hematein. The dominant complexes involved in the staining are hemalums: a mixture of the mordant dye, hematein, and a metal salt, aluminum alum.[4] The H solution is acidic on initial introduction into the tissue.[5] The hemalums have a high affinity for the chromatin, leaving the

Address all correspondence to: Adam Tuer, University of Toronto, Department of Chemical and Physical Sciences, 3359 Mississauga Road North, Mississauga, Ontario, L5L 1C6 Canada. Tel: 905-828-3808; Fax: 905-828-5425; E-mail: adam.tuer@utoronto.ca

1083-3668/2010/15(2)/026018/9/$25.00 © 2010 SPIE

nucleous, mitochondria, and ribosomes a purple color after staining. "Blueing" is then performed, by which the stained tissue is rinsed under alkaline solution causing the stain to transition to a blue hue.[5] Counterstaining is done with the fluorescent dye, eosin Y. As an anionic dye, eosin stains almost all proteins and, therefore, binds to nearly every structure present in the tissue.[1] Eosin marks the cytoplasm, connective tissue, collagen, and extracellular structures a pink color.

Nonlinear microscopy has been used to investigate H&E histological sections,[6] as well as tissue stained separately with H[6,7] and E dyes.[8] High third-harmonic signals originating from H-stained intracellular structures[6,7] have been observed. The strong THG signal from H was assigned[7] due to resonance enhancement at their excitation wavelength, 1230 nm. Investigations of E-stained tissue with MPF and fluorescence lifetime imaging microscopy (FLIM) were carried out previously.[8] Observation has shown that without the presence of hemalum, eosin stains the entire tissue.[8] While in the presence of hemalum, eosin fluorescence is present only in the extranuclear region.[6–8]

In this study, nonlinear imaging of stained histological sections was performed to elucidate the origin of nonlinear signals. The results revealed that strong THG originates due to the aggregation of hemalum complexes, with further enhancement due to an interaction with eosin. In addition, spectroscopic and lifetime measurements of eosin fluorescence showed efficient quenching by neutral hemalum complexes. The study provides the basis for future applications of nonlinear multicontrast microscopy for histological investigations and, in particular, for cancer imaging and diagnostics.

2 Methods

2.1 *Nonlinear Multicontrast Microscopy*

Structural investigations of histological sections were performed with a three-channel multicontrast nonlinear microscope using the photon-counting detection method to measure simultaneously MPF, SHG, and THG. Epidetection was used for MPF, while SHG and THG were detected in the forward direction. The setup is described in detail elsewhere.[9] Briefly, a home-built femtosecond $Yb:KGd(WO_4)_2$ oscillator was used for nonlinear excitation microscopic imaging. The laser provided ~430 fs pulses emitting at 1028 nm with a pulse repetition rate of 14.3 MHz.[10] A 40×1.3 numerical aperture (NA) oil immersion objective (Zeiss) was used for excitation, providing spatial resolution defined in terms of the full-width-at-half-maximum (FWHM) of 1.8 μm axially and 510 nm laterally. The axial resolution was measured using THG from a glass-air interface and the lateral resolution was deduced following Squier and Müller.[11] To capture 3-D images of 50 μm thick samples, a 20×0.75 NA air objective (Zeiss) was used to increase the available working distance (~400 μm), providing spatial resolution of 575 nm laterally and 3.5 μm axially, determined in a similar manner as for the oil objective. An OG530 (CVI Laser) and two BG39 (Schott) color glass filters were used for MPF collection, while bandpass filters 514 ± 10 and 340 ± 10 nm (CVI Laser) were used for SHG and THG, respectively. The images were obtained by scanning the sample with a 2 μs dwell time, and 50 to 300 frames of 128×128 pixels were summed to obtain an image. Pulse energies from 10 to 600 pJ at the sample were used during scanning.

2.2 *Spectrally Resolved Time-Correlated Single-Photon-Counting Microscopy*

A home-built temporally resolved nonlinear excitation laser scanning microscope was used for characterization of fluorescence lifetimes. The femtosecond $Yb:KGd(WO_4)_2$ oscillator was used for excitation. The excitation beam was expanded with a telescope to match the entrance aperture of a 20×0.75 NA microscope objective (Zeiss), and focused onto the sample with pulse energies from 20 to 500 pJ. The fluorescence signal was collected in the backward direction, reflected by a dichroic mirror (high reflection at 435 to 575 nm, Thorlabs), passed through a bandpass filter (525 to 630 nm, Semrock) and focused onto a R3809U-50 microchannel plate photomultiplier tube (MCP-PMT, Hamamatsu). For the spectrally resolved setup, the fluorescence signal was collected in the backward direction through a spectrometer (535 to 907 nm) (UTM131204-50, P&P Optica) onto a 16-channel multianode photomultiplier module (PML-16, Becker & Hickl GmbH). The two-photon excitation emission spectra were obtained from the normalized photon counts in each channel, with the channel wavelengths being calibrated from a known fluorescent species (coumarin 45) and 10 nm bandpass filters (FB520-10, FB530-10, FB550-10, FB570-10, FB590-10, FB610-10, Thorlabs). Fluorescence images were acquired with a SPC830 card (Becker & Hickl GmbH). The time-correlated single-photon-counting (TCSPC) method was employed for detection.[12] Time-resolved data were recorded for each pixel of the image. For imaging, the sample was translated by an *xyz*-piezoelectric translation stage (E-501, Physik Instrumente). Each pixel of a 128×128 image of MPF decays were fit with three exponential components for all the samples, with the exception of the unstained tissue sample. The unstained tissue sample was fit with two exponential components ($\tau_1=845\pm170$ ps, $a_1=61\pm6\%$, $\tau_2=3350\pm310$ ps, $a_2=39\pm6\%$). The average lifetime at each pixel was calculated for all stained tissue samples with the third component fixed at the average lifetime of the unstained tissue (1820 ± 130 ps). The equation for average lifetime is $\tau_{avg}=\Sigma_i a_i\tau_i/\Sigma_i a_i$, where a_i and τ_i denote the amplitude and lifetime of the different components, respectively. For each sample, a distribution of the average lifetime versus number of occurrences, not weighted to pixel intensity, in the image was fit with a Gaussian function. The $\pm$ in the stated average lifetimes corresponds to the bandwidth of the fitted Gaussian function. The FWHM of the MCP-PMT response was 70 ± 10 ps, which was used for the fitting algorithm of fluorescence decays in SPCImage (Becker & Hickl GmbH).

2.3 *Absorption Spectra*

The absorption spectra of solutions and tissues were recorded with an OLIS-14 (upgraded Cary-14) spectrophotometer. For the tissue absorption spectra, all samples were measured having an aperture of area 0.5 cm^2 placed in similar positions on the microscope slides. The absorption/scattering of the unstained tissue was subtracted from all spectra of the stained samples.

2.4 *Emission Spectra*

The emission spectra of tissues mounted on the microscope slides were recorded with a Quantamaster spectrofluorimeter (PTI). Normal incidence excitation light at 514 nm, provided by a xenon arc lamp, was used for illumination. The collection angle of fluorescence was at 45 deg with respect to the microscope slide, to reduce the collection of scattered excitation light. The autofluorescence spectrum of the unstained tissue sample was subtracted from all spectra of the stained samples. The emission spectra of solutions were recorded in a 10 mm optical glass cuvette, with a useable range of 320 to 2500 nm (9SOG-10, Starna Cells, Inc.), with excitation at normal incidence and fluorescence collection at 90 deg.

2.5 *Determination of the Second Hyperpolarizability* $\langle\gamma_{\mathrm{eff}}\rangle$

The THG ratio method was employed to determine the effective third-order susceptibility $\chi^{(3)}(3\omega)$ of the dyes in solution.[13,14] A modified setup of the nonlinear multicontrast microscope was used with a 0.25 NA objective. The $\chi^{(3)}(3\omega)$ determination method was based on procedure previously described,[13,14] using borosilicate cuvettes (W5010, VitroCom) and taking $n_{\mathrm{glass},\omega}=1.463$, $n_{n_{\mathrm{glass},3\omega}}=1.493$, and $\chi^{(3)}_{\mathrm{glass}}=2.07\times10^{-14}$ esu (obtained using Miller's rule and $\chi^{(3)}_{\mathrm{fused\ silica}}$ as a reference). The refractive indices of solutions were measured at 1028 and 343 nm using a home-made UV-NIR refractometer. The refractometer used a LH-450 xenon arc lamp (SLM Instruments) with a MC320/H monochromator (SLM Instruments) to select the desired wavelength. The light passed through two optical grade equilateral pure YAG prisms (Red Optronics), with two thin compartments between the prisms containing the solution of interest and water. The light was collected by a camera (CMOS), while the prisms were rotated until total internal reflection was observed in the solution compartment. The index of refraction of the solution was then calculated using water as a reference. Using the THG ratio method, the $\chi^{(3)}$ was measured for solutions at multiple concentrations and the second hyperpolarizability of the dye in solution was determined using a method described by Shcheslavskiy et al.[15]

2.6 *Tissue and Staining*

All animals were treated humanely in accordance to the Canadian Council of Animal Care Guidelines. The prostate tumor model TRAMP (TRansgenic Adenocarcinoma of Mouse Prostate) was used for the investigation as previously described.[16] A total of three TRAMP mice, 28 weeks of age, were used for the study. These mice were classified as having an advanced form of the disease. Tissue collected at necropsy were fixed in 4% paraformaldehyde overnight at 4 °C and then transferred to 70% ethanol prior to processing. Tissues were embedded in paraffin, sectioned at 5 to 50 μm thicknesses, and mounted on ProbeOn-Plus slides. The slides were stained with H (Surgipath #01562) and E (Surgipath #01602) dyes using standard procedure and covered with Aqua Poly-Mount (Polysciences Inc.) coverslips.[16] Four types of tissue samples were made: H-stained tissue, E-stained tissue, H&E-stained tissue, and a control sample (unstained). All four types of tissue sections originated from the same tissue sample.

2.7 *Solutions of Hematein-Aluminum Complexes and Eosin Y*

Standard solutions of eosin Y disodium salt (Sigma-Aldrich, 85.0%) were dissolved in distilled water and further diluted to appropriate concentrations.

To develop cationic hemalums ($HmAl^{+}$ and $HmAl^{2+}$), two standard solutions of hematein and aluminum were necessary. Initially, a 10^{-3} M standard solution of hematein was made by dissolving hematein (Fluka, grade for microscopy) in distilled water with the addition of a solubilizer, 3% v/v of anhydrous ethylene glycol (Sigma-Aldrich, 99.8%). A 10^{-3} M standard solution of aluminum was produced by dissolving aluminum ammonium sulfate dodecahydrate (Sigma-Aldrich, 99%) in the acetate buffer. An acetate buffer of 10^{-2} M at pH 4.7 was made by dissolving glacial acetic acid (J.T. Baker, 80%) and sodium acetate trihydrate (BDH, Inc., 99.5%) in distilled water. The two solutions were further diluted to appropriate concentrations. Hematein standard solution was added dropwise to aluminum standard solution to obtain a molar concentration ratio of 13.

To develop neutral hemalums ($HmAl^{0}$), two other standard solutions of hematein and aluminum were made analogous to the procedure for acidic hematein-aluminum solutions however; aluminum ammonium sulfate dodecahydrate was dissolved in an aqueous solution of disodium hydrogen orthophosphate anhydrous (BDH Inc., 99.0%) at a concentration of 10^{-2} M. The hematein and aluminum solutions were further diluted to concentrations ranging from 10^{-3} to 10^{-5} M. The pH of the hemalum solution was kept at pH 8.7 and the hematein standard solution was added dropwise to the aluminum standard solution to obtain a molar concentration ratio of 13.

3 Results

3.1 *Nonlinear Imaging*

Initially, four types of tissue sections were prepared: H-stained, E-stained, H&E-stained, as well as unstained tissue sample, to investigate the origins of MPF and THG. All samples were sectioned from the same tissue. Simultaneous images of the sections were collected using MPF, SHG, and THG contrast mechanisms with a multicontrast nonlinear microscope. High-magnification MPF and THG images showing an individual cell as well as larger area scans are presented in Fig. 1. SHG was generated predominantly from collagen, and showed no appreciable improvement in the presence of hemalum complexes or eosin (data not shown).

Surprisingly, in the H-stained tissue, MPF originated outside the nucleus [Figs. 1(a) and 1(b)], where hemalum complexes were thought not to bind. Overstaining with high concentrations of H and insufficient differentiation during the washing process could result in hemalum complexes binding to proteins outside the nucleus.[4] The MPF average lifetime was short (320 ± 25 ps) and the fluorescence intensity was relatively weak; nonetheless it was higher than the autofluorescence of the unstained sample. The autofluorescence (not shown) showed some cellular structure, such as cell borders, though it was only observable at much higher excitation powers than was required for stained tissue imaging.[6] THG of

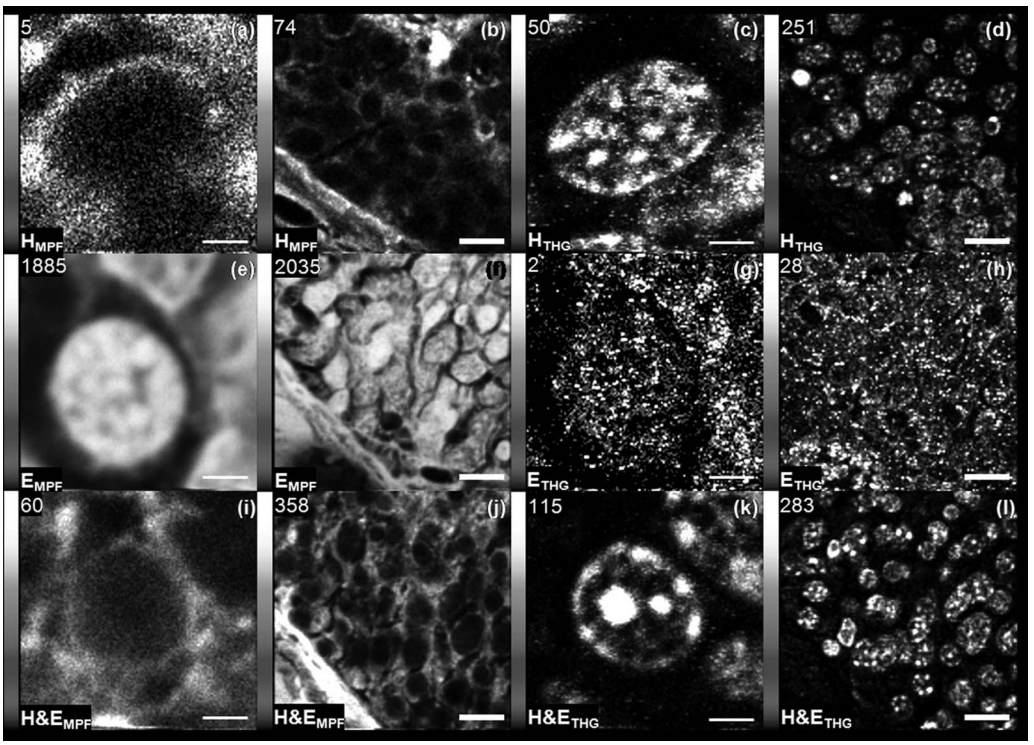

Fig. 1 Multicontrast imaging of stained TRAMP tissue with H and E dyes. MPF (two leftmost columns) and THG (two rightmost columns) images of H-stained tissue (a) to (d), E-stained tissue (e) to (h), and H&E-stained tissue (i) to (l). All images were obtained under the same imaging conditions. The rate of scanning was 10 frames/s, and images were obtained by summing 300 frames. The thin scale bar in high magnification images [(a), (c), (e), (g), (i) and (k)] is 3.5 μm, while the thick scale bar in lower magnification images [(b), (d), (f), (h), (j) and (l)] is 20 μm. The intensity scale bar to the left of each image indicates from 0 (black) to a maximum threshold (white) number of photons detected for a single pixel in the image. The pulse energy at the sample was approximately 100 pJ.

H-stained tissue originates almost exclusively from the nuclear regions [Figs. 1(c) and 1(d)]. The border of the nuclear membrane is clearly visualized in THG with both nuclei shape and size easily observable. Likely, the THG visualizes intracellular structures rich in nucleic acids, such as the nuclei, mitochondria, ribosomes, and nucleoli. Ribosomes and the nucleoli have been shown to be intricately linked to tumorigenesis,[17] as is nuclear size and shape. Thus, the ability to visualize these subcellular organelles inside of the 3-D tissue structure could lead to improvements in cancer diagnostics.

The signals collected from the E-stained tissue appeared to be the antithesis of the H-stained structures. The E-stained sample showed fluorescence over the entire tissue area [Fig. 1(f)], which is consistent with eosin being an anionic dye with an affinity for most proteins. The most intense MPF appeared in the nuclear regions [Figs. 1(e) and 1(f)], while regions exterior to the nucleus contained relatively lower photon counts. Nonetheless, regions outside the nucleus showed a higher level of counts than the H-stained fluorescence sample. A fast (295 ± 30 ps) average lifetime of the fluorescence was observed in the tissue, which is slightly shorter than in a previous investigation[8] (380 ± 162 ps), most probably due to the differences in tumor model (TRAMP compared to MCF10A), sample preparation, and instrument response (70 compared to 190 ps). The third-harmonic signal in the E-stained tissue showed little improvement compared to the control sample at low excitation powers; though some cellular structure is observable in THG images [Figs. 1(g) and 1(h)]. At approximately 1 nJ of pulse energy, THG was observed in the regions outside the nucleus. At this high laser power, the distribution of MPF and THG in the image was observed to be anticorrelated (data not shown).

In the H&E-stained tissue, MPF was weak from the nuclear regions, while strong in the regions outside the nucleus [Figs. 1(i) and 1(j)]. The high contrast of MPF intensity between the interior and exterior of the nuclear regions appears due to differences in the concentration of fluorescence molecules or fluorescence quenching properties in the two regions. The lifetimes of the MPF in the H&E-stained tissue were extremely short (115 ± 10 ps) compared to both the H-stained (320 ± 25 ps) and E-stained tissue (295 ± 30 ps), showing the presence of strong fluorescence quenching. Most intriguing was the high intensity third-harmonic signal generated from the nuclear regions of the tissue [Figs. 1(k) and 1(l)]. Even without accounting for the lower collection efficiency of the THG channel in the UV region, the third-harmonic signal was significantly stronger than SHG intensity from collagen (SHG image is not shown, see similar image in Tuer et al.[6]). The THG image of the H&E-stained tissue had structural features very similar to those of H-stained tissue, however the signal level was on average 2.5 times larger.

To investigate the 3-D structural organization, a 50 μm thick H&E-stained histological section (Fig. 2) was imaged with the multimodal nonlinear microscope. The MPF signal

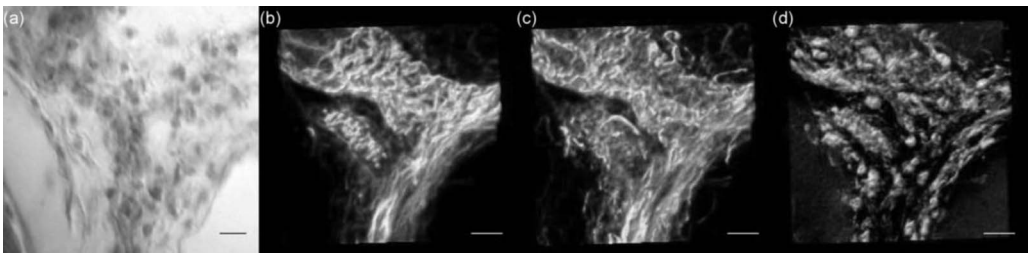

Fig. 2 (a) White light image of an H&E-stained histological section 50 μm thick with corresponding renderings of 3-D structure visualized with (b) MPF, (c) SHG, and (d) THG nonlinear contrast mechanisms. Imaging was performed with a 0.75 NA air objective. Each optical section was obtained by summing 20 image frames, and the optical sections were recorded at different depth with 1 μm step between them. The pulse energy at the sample was approximately 600 pJ. The scale bars for all images are 10 μm.

originating from the eosin stain highlights predominantly the connective tissue [Video 1(a)]. The SHG appears to correspond to collagen within the connective tissue, with no enhancement in intensity due to the presence of either the H or the E stain [Video 1(b)]. The corresponding THG signal highlights the nuclei revealing the locations of the cells within the tissue [Video 1(c)]. In addition, a weaker THG signal, although comparable to the strength of the tissue-glass interface, highlights the connective tissue, corresponding to various interfaces, mostly with collagen. The rich structural information revealed by each nonlinear contrast mechanism can be directly compared [Video 1(d)], aiding in better understanding about the spatial organization of the tissue.

3.2 *Spectroscopic Investigations*

To elucidate the origins of MPF and THG signals, absorption and fluorescence spectroscopic investigations were performed. Initially, linear absorption and fluorescence spectra of the dyes in solution were obtained. The absorption spectra of hemalum complexes were measured at pH 4.7 and pH 8.7 [Figs. 3(a) and 3(b)]. Fitting the spectra for pH 4.7 and pH 8.7 with multiple Gaussians produced peaks at 427, 509, 566 (572), and 633 nm (Table 1). In keeping with assignments provided by Bettinger and Zimmerman,[4,5] the 427 nm peak was assigned to hematein (Hm), while the hemalum complexes $HmAl^{2+}$, $HmAl^{+}$, and $HmAl^{0}$ were assigned 509, 566 (572), and 633 nm, respectively. The absorption spectra revealed that on changing to pH 8.7, the hemalum spectrum shifted to the red. The fits revealed that relative concentration of $HmAl^{0}$ complexes increased at the expense of $HmAl^{2+}$ and $HmAl^{+}$ complexes in the pH 8.7 solution.

There was no observable linear fluorescence from the hemalum solution at pH 4.7 and only very low nonlinear excitation fluorescence could be detected with the multiphoton excitation microscope. However, hemalum solution at pH 8.7 did show linear excitation fluorescence with a maximum at 536 nm [Fig. 3(d)]. For nonlinear excitation, the fluorescence dependence on the excitation intensity showed a two-photon process. Although, the nonlinear absorption of hemalum complexes is not known, the similarity of one- and two-photon excitation fluorescence spectra indicate that the $HmAl^{2+}$ absorbing at 509 nm is a two-photon fluorescent species in the pH 8.7 environment, but does not fluoresce in pH 4.7 solution. With the presence of two-photon absorption at a 1028 nm fundamental excitation wavelength, resonance enhancement of THG in the hemalum solutions was expected.[18]

The absorption spectrum of eosin was also measured in aqueous solution [Fig. 3(c)]. Fitting the spectra revealed peaks at 340, 497, and 517 nm. The 517 and 497 nm wavelengths correspond to the eosin monomer and dimer, respectively.[19] From the linear absorption spectrum of eosin, resonance enhancement of THG could be expected since the two peaks at 517 and 340 nm corresponds with double and triple the frequency of our excitation source, respectively.

The linear fluorescence spectrum of eosin aqueous solution is presented in Fig. 3(d), showing the maximum emission at 543 nm. Fluorescence emission from the eosin solution is also observed with nonlinear excitation at the fundamental wavelength of 1028 nm. The two-photon excitation fluorescence spectrum of E-stained tissue was measured with the spectrally resolved TCSPC microscope (Fig. 4), which corresponded to the linear fluorescence spectrum from the solution.

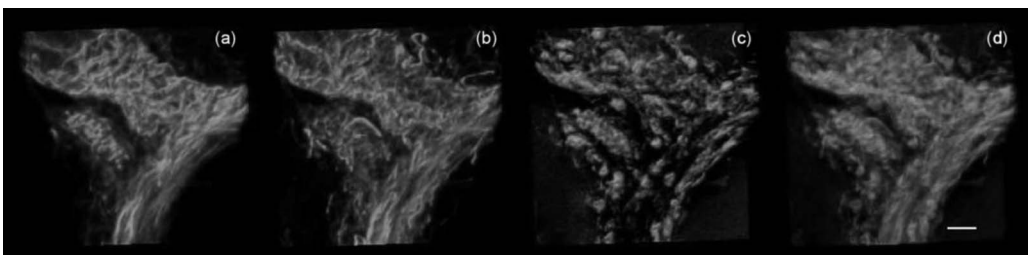

Video 1 Three-dimensional renderings of (a) MPF, (b) SHG, (c) THG, and (d) a composite structure from a 50-μm thick H&E-stained histological section. The imaging conditions are identical to that of Fig. 2. The composite structure (d) is colored MPF (red), SHG (green), and THG (blue), where overlap coloring follows the *RGB* standard color scheme. The scale bar is 10 μm (QuickTime, 4.57 MB). (Color online only.) [URL: http://dx.doi.org/10.1117/1.3382908.1].

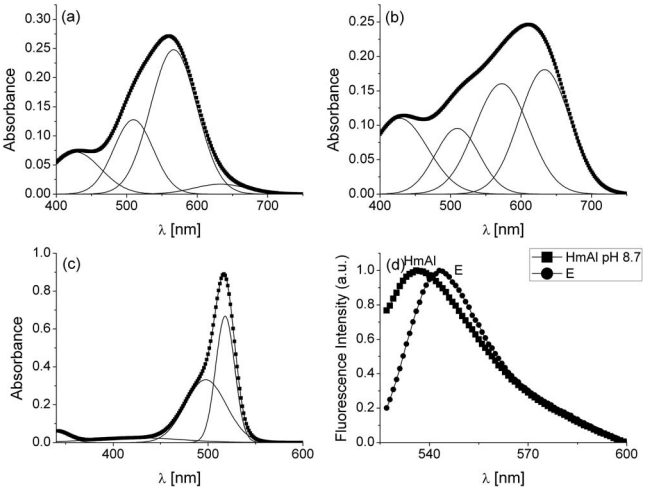

Fig. 3 Absorption and normalized fluorescence spectra of hemalums and eosin in solution. Absorption spectra of HmAl complexes in buffer solution at (a) pH 4.7 and (b) pH 8.7. Both solutions were made with a $[Hm]_{initial} = 4 \times 10^{-4}$ M and a molar concentration ratio between hematein and aluminum of 13. (c) Absorption spectrum of eosin at 10^{-5} M in aqueous solution. The absorption spectra were analyzed by fitting multiple Gaussians (solid lines). The reconstructed spectra from the multiple Gaussians (solid lines) closely correspond to the measured spectra (dots). (d) Normalized emission spectra of HmAl solution (8×10^{-4} M) at pH 8.7 (line with solid squares) and eosin (1.8×10^{-4} M) solution (line with solid dots).

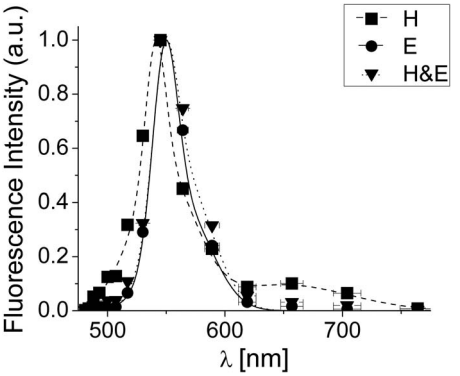

Fig. 4 Normalized two-photon excitation emission spectra of H-stained, E-stained, and H&E-stained tissue, obtained with an excitation wavelength of 1028 nm. The squares, circles, and triangles represent measured values, while the dashed, solid, and dotted lines represent the simulated emission spectra reconstructed by fitting multiple Gaussians to the measured data.

Power dependence measurements of eosin fluorescence intensity showed MPF to be a two-photon process (data not shown). Therefore, as was the case for hemalum solutions, resonance enhancement of THG for eosin was expected.

The absorption spectra of the stained tissue samples were then measured (Fig. 5). Fitting the absorption spectrum of the H-stained tissue [Fig. 5(a)] with multiple Gaussians revealed a number of hemalum complexes present in the tissue (Table 1). The fitted Gaussians peaked at 432, 528, 587, and 621 nm. Keeping with the previous assignments for hemalum complexes in solution, Hm, $HmAl^{2+}$, $HmAl^{+}$, $HmAl^{0}$ were assigned 432, 528, 587, and 621 nm, respectively. They correspond to the peak values of 445, 530, 595, and 615 nm previously reported[5] with H-stained HeLa cells.

The linear fluorescence spectrum of the H-stained tissue was observed to have a peak at 541 nm [Fig. 5(d)]. The nonlinear fluorescence spectrum of H-stained tissue revealed a similar peak at 545 ± 8 nm (Fig. 4); however, an additional peak around 657 ± 20 nm, with low intensity ($\sim 10\%$) compared to the 545 nm peak, was also observed (Fig. 4). Therefore, with excitation power dependency measurements indicating a two-photon process, the likely fluorescing hemalum complex in tissue is the $HmAl^{2+}$, emitting at 541 nm, with an observed linear absorption peak around 528 nm. Additionally, in the tissue there appears to be low-intensity nonlinear excitation fluorescence at 657 nm from either $HmAl^{+}$ or $HmAl^{0}$, which is one-photon forbidden. The measurements done in solution [Fig. 3(d)] also suggest that the $HmAl^{2+}$ is the fluorescent species in a basic pH 8.7 environment.

From the fits of the absorption spectra it is evident that $HmAl^{0}$ has the largest absorption amplitude and is not a major fluorescent species. With all hemalum complexes having

Table 1 Absorption maxima of dye species in solution and tissue.

	Solution λ_{max} (nm)			Tissue λ_{max} (nm)		
Complexes	HmAl pH 4.7	HmAl pH 8.7	E	H	E	H&E
Hm	427	427	—	432	—	432
$HmAl^{2+}$	509	509	—	528	—	(500–536)[a]
$HmAl^{+}$	566	572	—	587	—	577
$HmAl^{0}$	633	633	—	621	—	628
E_{mono}	—	—	517	—	536	536
E_{dimer}	—	—	497	—	500	500

[a]The peak could not be differentiated from the E_{mono} and E_{dimer} absorption peaks.

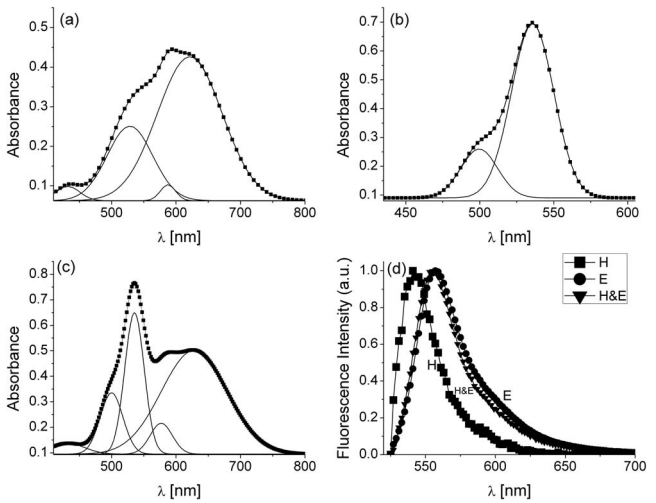

Fig. 5 Fitted absorption spectra of (a) H-stained, (b) E-stained, and (c) H&E-stained TRAMP tissue sections, respectively, and (d) normalized emission spectra of H-stained, E-stained, and H&E-stained histological sections. The fits to absorption spectra and Gaussian components are shown with solid lines, while measured spectra are shown with dots.

comparable extinction coefficients[4] it follows that $HmAl^0$ is the most abundant species. Therefore, as hemalum accumulates mostly in the nuclei, where no fluorescence is observed with H staining [Figs. 1(a) and 1(c)], the dominant species binding to the chromatin is likely $HmAl^0$. This is the first indication that $HmAl^0$ is responsible for the generation of the third-harmonic in the H-stained tissue.

The absorption spectrum of E-stained tissue [Fig. 5(b)] reveals some dimerization of eosin molecules.[19,20] The highest aggregated complex of eosin is its dimer, which does not fluorescence.[20] The absorption peaks observed in the tissue are red-shifted compared to the aqueous solution, which is in good agreement with previous reports.[21] The linear [Fig. 5(d)] and nonlinear (Fig. 4) excitation fluorescence spectra of E-stained tissue peak at 557 nm, which are consistent with what has been previously reported.[21] The nonlinear excitation fluorescence closely corresponds to the linear fluorescence spectrum and is red shifted compared to the nonlinear fluorescence from H-stained tissue (Fig. 4).

The absorption spectrum of the H&E-stained tissue [Fig. 5(c)] appears to be an average combination of the H-stained and E-stained spectra. However, there is an additional shift in the spectrum around 640 nm, which could possibly be due to an interaction between hemalum complexes and eosin. The emission spectrum from the H&E-stained tissue closely resembled fluorescence of E-stained tissue for both linear [Fig. 5(d)] and nonlinear excitation (Fig. 4). The $HmAl^{2+}$ fluorescence at 541 nm was no longer observable most likely due to fluorescence quenching by eosin. Also, the linear absorption band from $HmAl^{2+}$ could not be differentiated from the bands of eosin.

With the previously observed shortening of the lifetime and the reduction in fluorescence intensity in H&E-stained compared to E-stained tissue, there is indication of eosin fluorescence quenching by hemalum complexes. The obvious spectral overlap between eosin emission and hemalum complexes, with absorption peaks at 587 ($HmAl^+$) and 621 nm ($HmAl^0$), supports this claim.

In conclusion, the spectroscopic investigations presented in this section show that in H&E-stained tissue, the eosin fluorescence is observed in the regions exterior to the nucleus, while the $HmAl^{2+}$ fluorescence appears to be quenched by transferring excitation energy to eosin monomer. In contrast, the fluorescence is not observed in the nucleus, because $HmAl^+$ and $HmAl^0$ complexes, which are only weakly fluorescent, quench eosin fluorescence. The fluorescence quenching suggests that eosin and hemalum complexes are present in the tissue within the Förster radius.

Table 2 Third-order nonlinear susceptibilities and second hyperpolarizibilities of hemalums and eosin measured with a 1028 nm excitation wavelength.

	Refractive indices		Nonlinear Properties	
Substance	n_ω	$n_{3\omega}$	$\chi^{(3)}$ (10^{-14} esu)	$\langle\gamma\rangle$ (10^{-32} esu)
[a]$HmAl^{+,2+}$	1.313	1.323	1.3±0.7	2.0±2.0
[b]$HmAl^0$	1.316	1.329	2.0±0.6	—
[c]E	1.327	1.353	2.2±0.3	1.8±1.4

[a]The HmAl solution at pH 4.7.
[b]The HmAl solution at pH 8.7. $HmAl^0$ measurement was performed on a sample with $[Hm]_{initial}=10^{-3}$ M.
[c]The susceptibility was measured at a $[E]_{initial}=4\times10^{-5}$ M.

3.3 *Investigations of Third-Order Nonlinearities*

Third-order nonlinear susceptibility measurements were performed in the nonlinear multicontrast microscope by the method, which makes use of the THG ratio between the signals at solution-glass and glass-air interfaces[13–15] (see materials and methods). The aqueous eosin solutions at multiple concentrations between 0 and 10^{-5} M were measured in order to calculate the second hyperpolarizability.[15] Likely, this range of concentration corresponds to the eosin monomer, as above 6×10^{-5} M a dramatic drop in the susceptibility was observed, possibly due to the increased concentration of dimers. The effective second hyperpolarizability for eosin was 1.8×10^{-32} esu (Table 2). This very large value is likely due to resonance enhancement, corresponding to the double frequency of our excitation source. This value is comparable to the second hyperpolarizability of carotenoid reported by Marder et al.[22] (1×10^{-32} esu) but is at least an order of magnitude larger than most reported organic molecules.[23]

Measurements of the second hyperpolarizibilities of the hemalum complexes in solution were performed at pH 4.7 and pH 8.7 (Table 2). The effective second hyperpolarizability of hemalum (HmAl) complexes in solution at pH 4.7 was determined to be 2×10^{-32} esu. This value of the second hyperpolarizability, like eosin, is large and is most easily reasoned by resonance enhancement.[7] Similar values for other organometallic compounds having second hyperpolarizibilities as high as 3×10^{-32} esu were reported.[23,24] Although the second hyperpolarizability of HmAl complexes was large, it alone could not explain the strong THG in tissue, since eosin has a comparably large hyperpolarizability and only slight increase in

THG signal could be observed compared to unstained tissue [see Figs. 1(g) and 1(h)]. While measuring the HmAl solution, it was noticed that upon "blueing," by shifting the pH to 8.7, stable blue precipitates were formed. Aggregate formation was observed at pH values as low as 6. These blue precipitates, which were previously observed,[5] exhibited strong THG and low MPF. Therefore, they are the most likely candidates for generating third-harmonic signal in the nuclear regions of the H-stained tissue. After filtration, the remaining solution containing $HmAl^0$ monomers was found to have an effective $\chi^{(3)}$ of 2×10^{-14} esu (Table 2). Unfortunately, second hyperpolarizability values could not be deduced due to uncertainty in concentration measurements of the blue precipitate solutions. However, an intensity ratio of the third-harmonic generated from the blue aggregates compared to an air-glass interface was measured to be 2.0 ± 0.8. The ratio is much larger than the ratio from eosin solution (0.029 ± 0.007) and HmAl pH 8.7 solution (0.038 ± 0.005) without aggregation. The HmAl complexes in tissue are in a dried environment; filtering the $HmAl^0$ aggregates from the solution and allowing them to dry on a microscope slide increased the THG ratio compared to an air-glass interface to 14 ± 6. The large ratio increase appears mostly due to significant differences in the refractive indices and third-order susceptibilities between dry and aqueous environments. The dried aggregates mimic well the strength of THG signal from the H-stained tissue.

These results indicate that staining the tissue with acidic H solution, promotes high concentrations of charged hemalum complexes to migrate to the compartments with negatively charged DNA and RNA via Coulomb interactions. On "blueing," the pH becomes basic initiating the conversion of hemalums to the neutral form, $HmAl^0$, and induces aggregation of the complexes, which exhibit strong generation of the third-harmonic inside the cells.

The THG intensity from H&E-stained tissue was appreciably larger than from H-stained tissue. Comparing the ratio of the third-harmonic generated from the stained cells to an air-glass interface for all tissue samples, revealed the measured ratios of 80 ± 53, 34 ± 9, 1.6 ± 0.1, and 0.25 ± 0.1 for the H&E-stained, H-stained, E-stained, and unstained tissue samples, respectively. We mimicked H&E tissue staining with H and subsequently with E by using $HmAl^0$ precipitates mixed with eosin dye ($30\ \mu L$ of $[E]=1.2\times10^{-4}$ M) and dried on a microscope coverslip. The THG was enhanced twofold compared to dried $HmAl^0$ precipitates, with the signal ratio being 28 ± 3. A weak anticorrelation between the THG of the $HmAl^0$ aggregates and MPF from eosin was observed, which is consistent with MPF and THG anticorrelation in H&E stained tissue [Figs. 1(i) and 1(l)]. The twofold enhancement of THG most probably originates due to an interaction between the hemalum complexes and eosin at the surface of $HmAl^0$ precipitates. Anticorrelation of fluorescence and THG also indicates that interacting eosin molecules are nonfluorescent. The THG observed in H- and H&E-stained tissue are stronger than in dried precipitates most probably due to differences in refractive index and nonlinear susceptibility of the tissue environment, and interaction of the dyes with chromatin. In addition, binding to DNA and RNA might induce more ordered aggregation/crystallization of the HmAl complexes and eosin resulting in a larger third-order susceptibility value.

The presented results point to the importance of molecular aggregates in serving as harmonophores for nonlinear microscopy. The control of the aggregation process during "blueing" might further increase the THG signal strength of the dyed histological sections and help to improve the method for diagnosing cancer at a single cell level.

4 Conclusion

We determined experimentally some of the nonlinear properties of the dominant hemalum complexes involved in H&E staining. The results suggest that THG observed in the H-stained tissue is due to aggregation of neutral hemalum complexes, while additional enhancement of the signals in H&E-stained tissue appears due to the interaction of neutral hemalum aggregates with eosin. Fluorescence lifetime and spectral measurements of H&E-stained tissue reveal quenching of $HmAl^{2+}$ fluorescence by eosin in the regions exterior to the nucleus, while the absence of fluorescence inside the nucleus is attributed to the quenching of eosin MPF by $HmAl^+$ and $HmAl^0$ complexes, as well as the formation of $HmAl^0$ aggregates. Imaging with multiple nonlinear contrast mechanisms is highly beneficial for revealing 3-D structures in the tissue microenvironment. Specifically in THG, the nuclear structures of cells may be readily visualized. This imaging capability may prove to be highly valuable in aiding to determine structural changes, on the cellular and tissue level, which correspond to cancer development and progression.

Acknowledgments

This work was supported in part by the Natural Sciences and Engineering Research Council of Canada, the Ontario Centre of Excellence for Photonics, the Canada Foundation for Innovation, and the Ontario Innovation Trust.

References

1. J. A. Kiernan, *Histological and Histochemical Methods*, 3rd ed., Butterworth Heinemann, Woburn, MA (1999).
2. R. Carriles, D. N. Schafer, K. E. Sheetz, J. J. Field, R. Cisek, V. Barzda, and J. Squier, "Imaging techniques for harmonic and multiphoton absorption fluorescence microscopy," *Rev. Sci. Instrum.* **80**, 081101 (2009).
3. R. Cisek, N. Prent, C. Greenhalgh, D. Sandkuijl, A. Tuer, A. Major, and V. Barzda, "Multicontrast nonlinear microscopy," in *Biochemical Applications of Nonlinear Spectroscopy*, V. V. Yakovlev, Ed., pp. 71–102, CRC Press, Boca Raton, FL (2009).
4. C. Bettinger and H. Zimmerman, "New investigations on hematoxylin, hematein, and hematein-aluminum-complexes. II. Hematein-aluminum complexes and hemalum staining," *Histochemistry* **96**, 215–228 (1991).
5. C. Bettinger and H. Zimmerman, "New investigations on hematoxylin, hematein, and hematein-aluminum-complexes. I. Spectroscopic and physico-chemical properties of hematoxylin and hematein," *Histochemistry* **95**, 279–288 (1991).
6. A. Tuer, L. Bakueva, R. Cisek, J. Alami, D. J. Dumont, J. Rowlands, and V. Barzda, "Enhancement of third-harmonic contrast with harmonophores in multimodal non-linear microscopy of histological sections," *Proc. SPIE* **6860**, 686005 (2008).
7. C. Yu, S. Tai, C. Kung, W. Lee, Y. Chan, H Liu, J. Lyu, and C. Sun, "Molecular third-harmonic-generation microscopy through resonance enhancement with absorbing dye," *Opt. Express* **33**, 387–389 (2008).
8. M. W. Conklin, P. P. Provenzano, K. W. Eliceiri, R. Sullivan, and P. J. Keely, "Fluorescence lifetime imaging of endogenous fluorophores in

histopathology sections reveals differences between normal and tumor epithelium in carcinoma in situ of the breast," *Cell Biochem. Biophys.* **53**, 145–157 (2009).
9. C. Greenhalgh, N. Prent, C. Green, R. Cisek, A. Major, B. Stewart, and V. Barzda, "Influence of semicrystalline order on the second-harmonic generation efficiency in the anisotropic bands of myocytes," *Appl. Opt.* **46**, 1852–1859 (2007).
10. A. Major, D. Sandkuijl, and V. Barzda, "Efficient frequency doubling of a femtosecond Yb:KGW laser in a BiB3O6 crystal," *Opt. Express* **17**, 12039–42 (2009).
11. J. Squier and M. Müller, "High resolution nonlinear microscopy: a review of sources and methods for achieving optimal imaging," *Rev. Sci. Instrum.* **72**, 2855–2867 (2001).
12. W. Becker, *The bh TCSPC Handbook*, 3rd ed., Becker & Hickl GmbH, Berlin (2008).
13. G. O. Clay, A. C. Millard, C. B. Schaffer, J. Aus-der-Au, P. S. Tai, J. A. Squier, and D. Kleinfeld, "Spectroscopy of third-harmonic generation: evidence for resonances in model compounds and ligated hemoglobin," *J. Opt. Soc. Am. B* **23**, 932–950 (2005).
14. J. M. Schins, T. Schrama, J. A. Squier, G. J. Brakenhoff, and M. Müller, "Determination of material properties by use of third-harmonic generation microscopy," *J. Opt. Soc. Am. B* **19**, 1627–1634 (2001).
15. V. Shcheslavskiy, G. I. Petrov, S. Saltiel, and V. V. Yakovlev, "Quantitative characterization of aqueous solutions probed by the third-harmonic generation microscopy," *J. Struct. Biol.* **147**, 42–29 (2004).
16. N. Greenberg, F. DeMayo, M. Finegold, D. Medina, W. Tilley, J. Aspinall, G. Cunha, A. Donjacour, R. Matusik, and J. Rosen, "Prostate cancer in a transgenic mouse," *Proc. Natl. Acad. Sci. U.S.A.* **92**, 3439–3443 (1995).
17. L. Montanaro, D. Trere, and M. Derenzini, "Nucleolus, ribosomes, and cancer," *Am. J. Pathol.* **173**, 301–310 (2008).
18. P. N. Butcher and D. Cotter, *The Elements of Nonlinear Optics*, Cambridge University Press, Avon, U.K. (1990).
19. G. R. Jones, D. A. Duddell, D. Murray, R. B. Cundall, and R. Catterall, "Eosin Y-macromolecule complexes, Part 1. Application of exciton theory to the study of the arrangement of eosin Y molecules in polycation-induced eosin Y dimers," *J. Chem. Soc., Faraday Trans. 2* **80**, 1181–1199 (1984).
20. G. R. Jones, R. B. Cundall, D. Murray, and D. A. Duddell, "Eosin Y-macromolecule complexes, Part 2. Interactions between eosin Y and polycations, a cationic surfactant and proteins," *J. Chem. Soc., Faraday Trans. 2* **80**, 1201–1213 (1984).
21. C. Y. Fu, U. S. Dinish, B. K. Ng, V. M. Murukeshan, L. K. Seah, and S. K. Lim-Tan, "Fluorescence lifetime imaging of haematoxylin and eosin-stained cervical tissue," in *Proc. Int. Conf. on Biomedical and Pharmaceutical Engineering*, pp. 368–372 (2006).
22. S. R. Marder, W. E. Torruellas, M. Blanchard-Desce, V. Ricci, G. I. Stegeman, S. Gilmour, J.-L. Bredas, J. Li, G. U. Bublitz, and S. G. Boxer, "Large molecular third-order optical nonlinearities in polarized carotenoids," *Science* **276**, 1233–1236 (1997).
23. R. R. Tykwinski, U. Gubler, R. E. Martin, F. Diederich, C. Bosshard, and P. Gunter, "Structure-property relationships in third-order nonlinear optical chromophores," *J. Phys. Chem. B* **102**, 4451–4465 (1998).
24. T. Bjornholm, "Development of molecules for all-optical switching devices," *Isr. J. Chem.* **36**, 349–356 (1996).